

# NeOTF: Speckle-Constrained OTF Neural Representation for Non-invasive Imaging through Scattering Medium

YUNONG SUN,<sup>1,\*</sup>

<sup>1</sup>University of California Irvine, Irvine, CA

\*yunongs1@uci.edu

**Abstract:** Imaging through scattering media via speckle correlation is fundamentally challenged by ill-posed reconstruction. To overcome this, we bypass direct object recovery and instead target the system’s deterministic optical transfer function (OTF). We introduce NeOTF, a framework that learns an implicit neural representation of the OTF. By optimizing this representation using multi-frame speckle intensities and a physical Fourier-domain prior, NeOTF robustly retrieves the system’s OTF. Subsequent deconvolution with this retrieved OTF yields high-fidelity object reconstructions. Both simulations and experiments demonstrate that NeOTF achieves superior accuracy and efficiency over conventional methods, establishing it as a practical solution for real-time scattering imaging.

## 1. Introduction

Imaging through scattering media is widely used in deep tissue imaging, lidar and astronomical imaging [1,2]. The methods for imaging through strong scattering include wavefront shaping [3–6], transmission matrix [7,8], time-of-flight [9,10] and memory effect [11,12]. Among these methods, scattering imaging technology based on memory effect and speckle correlation can efficiently achieve non-invasive scattering imaging without additional optical components. Due to the poor robustness of the phase retrieval [13] and its difficulty in recovering objects with complex structure, other improved phase retrieval algorithms have been proposed [14–17]. They usually improve the convergence speed and imaging quality by adding spatial domain constraints or prior information. In addition, thanks to the prior of data distribution and the powerful fitting ability of neural networks, neural networks have also been used in the task of phase retrieval or image reconstruction, and significantly improved the imaging quality.

Data-driven neural networks perform well on specific data [18,19]. Due to the lack of a large number of different scenes and target data, its generalization and transfer learning capabilities are poor, which limits its application in practical scenarios. Model-driven neural networks use loss function optimization based on physical models instead of paired data sets [20–24], which greatly improve the ability of generalization. Although some methods have been proposed to improve network convergence speed and image quality [21,25,26], this type of model necessitates numerous iterations to optimize each of the speckles separately, which is a process known to be time-intensive in dynamic imaging.

In this paper, a non-invasive scatter imaging algorithm named NeOTF, which is based on implicit neural representation [27–30] of optical transfer function (OTF) is proposed. This method retrieves the OTF of the scatter imaging system within the memory effect by the speckle constraints in Fourier domain. The proposed method outperforms the traditional phase retrieval algorithm and untrained neural network method in terms of imaging quality and efficiency.

## 2. Methods

### 2.1. Physics model and constraints

Within the memory effect, the speckle intensity formed by the light emitted by the object after passing through the strong scattering medium can be regarded as the convolution form of the

intensity image of the object and the point spread function (PSF) of the imaging system on the depth plane of the object [11],

$$I = O * S, \quad (1)$$

where  $I$  and  $O$  are the intensity of speckle and object, respectively.  $S$  is the PSF of the imaging system. As Fig.1(a) shows, the invasive scattering imaging method can directly reconstruct the object by measuring the PSF and deconvolution. In non-invasive speckle correlation scattering imaging, as shown in Fig.1(b), the autocorrelation of objects can be estimated from the autocorrelation of speckles [12].

$$I \star I = (O \star O) * (S \star S) \approx O \star O, \quad (2)$$

where  $S \star S$  can be considered as a Dirac function in ideal experimental setup due to the characteristics of random speckles.

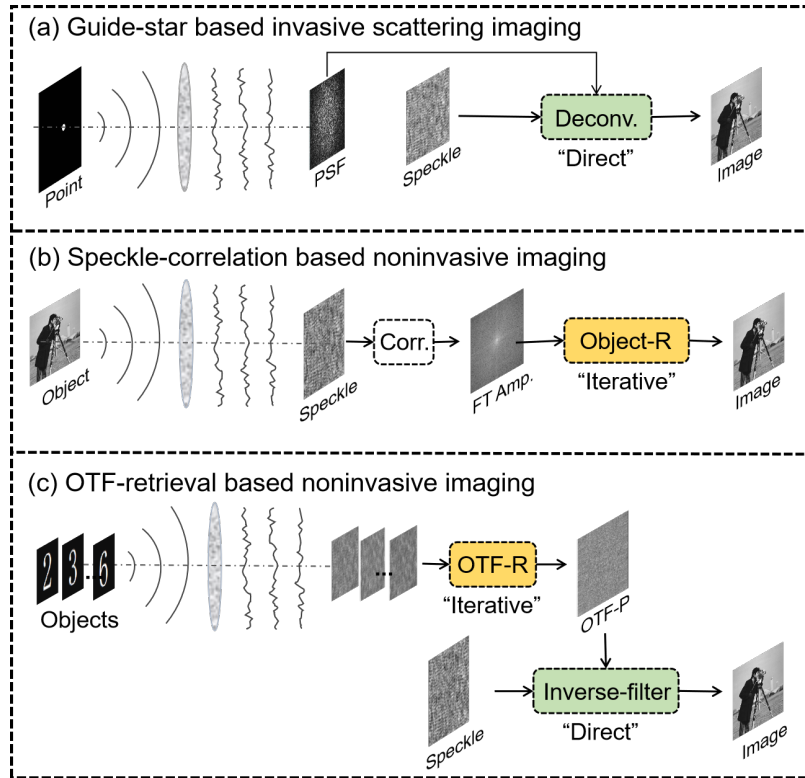


Fig. 1. Illustration of memory effect scattering imaging method. (a) represents guide-star based invasive scattering imaging. The images are directly recovered by the deconvolution with the PSF calibrated from the point source. (b) is Sepckle-correlation based noninvasive imaging. The images are reconstructed from the Fourier amplitude of speckle with phase retrieval algorithm. (c) shows OTF-retrieval based noninvasive imaging. The phase of OTF is retrieved from the speckles with iterative algorithm. And image can be directly restored from the speckle by inverse-filtering.

Fig.1(c) presents another method to achieve non-invasive imaging, which combines the iterative phase retrieval process and direct inverse-filtering [31–33].

According to Eq.(1), the Fourier transform of the object can be expressed by the following

equation:

$$\mathcal{F}(O) = \frac{\mathcal{F}(I)}{\mathcal{F}(S)} = \frac{|\mathcal{F}(I)|}{|\mathcal{F}(S)|} e^{i(\phi_I - \phi_S)}, \quad (3)$$

where  $\mathcal{F}(\cdot)$  denotes the function of Fourier transform,  $\phi_I$  and  $\phi_S$  are the Fourier phase of  $I$  and  $S$ , respectively. It has been reported that  $|\mathcal{F}(S)|$  acts as a low-pass filter in imaging and  $\phi_S$  can be used to recover the object without  $|\mathcal{F}(S)|$  [33, 34]. So the Eq.(3) can be considered as,

$$\mathcal{F}(O) \approx \mathcal{F}(O') = |\mathcal{F}(I)| e^{i(\phi_I - \phi_S)}, \quad (4)$$

where  $O'$  represents the low-pass filtered version of  $O$  due to the diffraction limitation. After imposing constraints on results, object's intensity in space domain can be expressed as,

$$O' = \text{RN} \left( \mathcal{F}^{-1}(\mathcal{F}(O)) \right), \quad (5)$$

where  $\mathcal{F}^{-1}(\cdot)$  denotes the function of inverse Fourier transform and  $\text{RN}(\cdot)$  represent the object domain constraints, which contain constraints of *Support Region* and *Real and Non-negative* [13].

According to the physics model mentioned above, the Fourier amplitude of diffraction-limited object  $|\mathcal{F}(O')|$  can be regarded the same as the Fourier amplitude of speckle  $|\mathcal{F}(I)|$ . The loss function of the neural network can be expressed as,

$$L = \| |\mathcal{F}(O')| - |\mathcal{F}(I)| \|_1, \quad (6)$$

where  $\| \cdot \|_1$  denotes the  $L_1$  normalization function.

## 2.2. Implicit neural representation for OTF retrieval.

The imaging pipeline and specific architecture of NeOTF is shown in Fig.2. The architecture of neural network is a simple multilayer perceptron with frequency encoder layer and SIREN activation function [27, 35], as illustrated in Fig.2(b). There are 3 hidden layer inner the NeOTF with 256 units in each layer and an activation function is used to map the output range to  $(-\pi, \pi)$ . Comparing with the network based on deep image prior [36, 37], implicit neural representation is more flexible and can be used to handle multiple inputs of different sizes without additional adjustment to the architecture. Similarly to the common implicit neural representation in the two-dimensional domain, the input of the network is the coordinate in two-dimensional frequency domain, and the output is the phase value at that frequency point. It is worth noting that the phase of the OTF in the scatter imaging system usually exhibits a statistical distribution similar to random noise. To help retrieve the random phase, we apply a frequency encoder layer and a SIREN activation function to overcome the problem that the output of INR is too smooth in the frequency domain. The phase map generated by the optimized network's OTF output is directly applicable for reconstructing the object from the speckle. This reconstruction process involves twice Fourier transforms and once inverse filtering. Furthermore, owing to the time-invariant nature of the OTF in a static scattering medium, a pre-optimized NeOTF model can be directly utilized to synthesize or reconstruct speckle patterns for novel objects without requiring any re-optimization.

As the algorithm diagram shows in the Fig.(2)(a), the framework starts with an initial parameter  $\theta_0$  for neural network, which output the phase of OTF  $\phi_s$ , and keeps updating in the training epochs. In each epoch, the multiple frames are successively used to update the guessed OTF's phase:

- (a) Calculate the intensity of objects by applying a forward process based on the physics model and constraints:

$$O_i = \text{Forward}(\mathcal{F}(I_i), \phi_S). \quad (7)$$

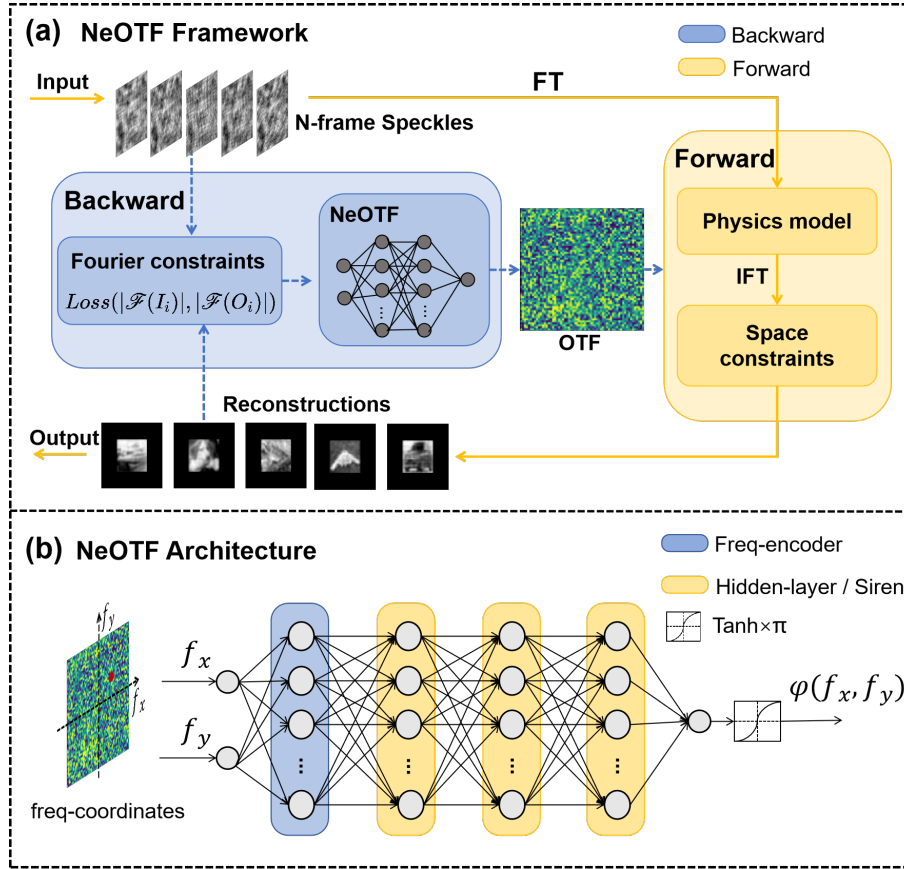


Fig. 2. (a) Schematic of NeOTF optimization and image reconstruction. The optimization begins with a multi-frame or single-frame speckle intensity image as input, ultimately yielding the reconstructed object intensity image derived from the corresponding speckle data. The yellow solid line indicates the image reconstruction, while the blue dotted line depicts the OTF retrieval. (b) The network architecture of NeOTF. It consists of a frequency encoding layer, three hidden layers with SIREN activation function, and an output layer with tanh activation function. The input is coordinates of  $(f_x, f_y)$ , and the output  $\phi(f_x, f_y)$  is the phase corresponding to the  $(f_x, f_y)$ .

- (b) Calculate the loss function designed between the Fourier amplitude of the intensity of the speckle  $I_i$  and the retrieved object  $O_i$ :

$$L_i = \text{Loss}(|\mathcal{F}(I_i)|, |\mathcal{F}(O_i)|). \quad (8)$$

- (c) Repeat step (a) to (b) with the  $i = i + 1$  until all the frames are used.

- (d) Sum up the loss among  $i$  frame speckles and update the parameters  $\theta'$  of neural network with Adam optimizer:

$$\theta' = \text{Adam}\left(\sum L_i, \theta\right). \quad (9)$$

- (e) Generate OTF's phase with updated neural network:

$$\phi_s(f_x, f_y) = \text{Model}_{\theta'}(f_x, f_y). \quad (10)$$

(f) Repeat step (a) to (e) until the criterion of convergence is reached.

Here, Forward  $(\cdot)$  represents the physics model and constraints, which shows the reconstruction from speckles to objects. Loss  $(\cdot)$  is the  $L_1$  loss function of Fourier amplitude. Adam  $(\cdot)$  is the adaptive moment estimation optimizer used in updating parameters of neural network. Model $_{\theta}$   $(\cdot)$  is inference of neural network with parameters of weight  $\theta$ .

### 3. Results

#### 3.1. Simulations

In order to explore the imaging effect of the proposed NeOTF model, we simulated speckled images in the same static memory effect scattering imaging system based on five natural images in CIFAR-10 dataset. The PSF of a scattering imaging system is an intensity image obtained by simulating the diffraction of an incoherent point light source through a limited aperture and random phase modulation of a scattering medium. The scattering speckle of an object is the convolution of the original image and the PSF. We perform a noise-free numerical simulation of NeOTF to verify the restoration results of the random phase transfer function and the quality of recovered image. The OTF of the system was determined by a circle aperture function with random phase. The simulated speckle is the intensity distribution of the object after passing through the OTF.

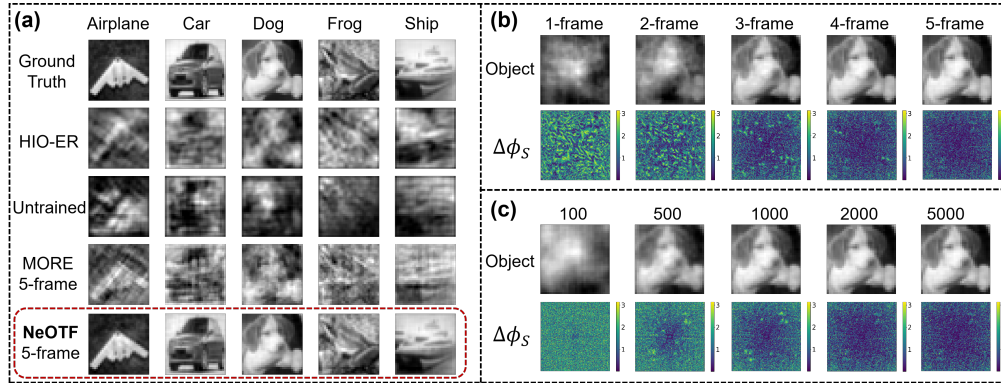


Fig. 3. Numerical simulations of NeOTF in non-invasive imaging through scattering medium. (a) is the object reconstruction with different algorithms. "GT" represent the diffraction-limited images of several natural images. (b) is the imaging result and OTF phase error of NeOTF when the input frame number is 1 to 5 frames and the iterations is set to 10,000 times.  $\Delta\phi_S$  is the residual map between the recovered OTF and ground truth, where the smaller the value, the smaller the phase difference. (c) is the imaging results of 'Dog' and OTF phase error of 5-frame NeOTF at 100~10000 iterations.

We compared the reconstruction results of several different methods for the same speckle, including HIO-ER, untrained neural network, *MORE* [33] and the NeOTF we proposed. We use a simple U-Net [38] as the backbone of the untrained neural network, and it is optimized by the  $L_1$  loss function in the Fourier domain. The input frame of NeOTF is set to 5 frames, so dose the *MORE*. All the algorithm were iterated for a sufficient number of rounds until convergence with the same speckles.

The comparison results are shown in Fig.3 and Tab.1. For speckle in natural images with high frequency components, the HIO-ER and untrained neural network methods based on single-shot speckle correlation are difficult to restore reliable results. The SSIM of the images they restored are basically less than 0.5, which can be regarded as unrecognizable. *MORE* and NeOTF

algorithm, which based on multi-frame speckle constraints and OTF retrieval, perform much better results than the single-shot reconstruction methods. They can achieve SSIM index of more than 0.5 on these images. Moreover, the SSIM index of 5-frame NeOTF reaches more than 0.9, and the reconstruction quality is better than the *MORE* algorithm based on traditional optimization. This is because phase retrieval is an ill-posed problem, and multi-frame speckles introduce strong physical constraints into the iterations, which can effectively improve the convergence of the algorithm and reduce errors. Intuitively, when more redundant speckles are input to the algorithm, the accuracy of the phase retrieval algorithm and the final image quality will also improve.

Table 1. Quantitative comparison of imaging quality with different speckle reconstruction algorithms and different numbers of input frame in NeOTF. Object-R and OTF-R represent object retrieval and OTF retrieval algorithms, respectively.

| Methods  |             | PSNR (dB) $\uparrow$ |       |       |        |        | SSIM $\uparrow$ |       |       |        |        |
|----------|-------------|----------------------|-------|-------|--------|--------|-----------------|-------|-------|--------|--------|
|          |             | "Air."               | "Car" | "Dog" | "Frog" | "Ship" | "Air."          | "Car" | "Dog" | "Frog" | "Ship" |
| Object-R | HIO-ER      | 12.4                 | 12.6  | 14.0  | 11.7   | 10.3   | 0.309           | 0.487 | 0.512 | 0.221  | 0.184  |
|          | Untrain     | 12.3                 | 6.92  | 8.86  | 13.6   | 7.80   | 0.284           | 0.06  | 0.242 | 0.316  | 0.213  |
| OTF-R    | <i>MORE</i> | 14.5                 | 13.7  | 16.4  | 16.5   | 14.4   | 0.531           | 0.568 | 0.713 | 0.635  | 0.583  |
|          | NeOTF       | 24.3                 | 19.8  | 22.7  | 21.1   | 19.4   | 0.88            | 0.90  | 0.93  | 0.93   | 0.84   |

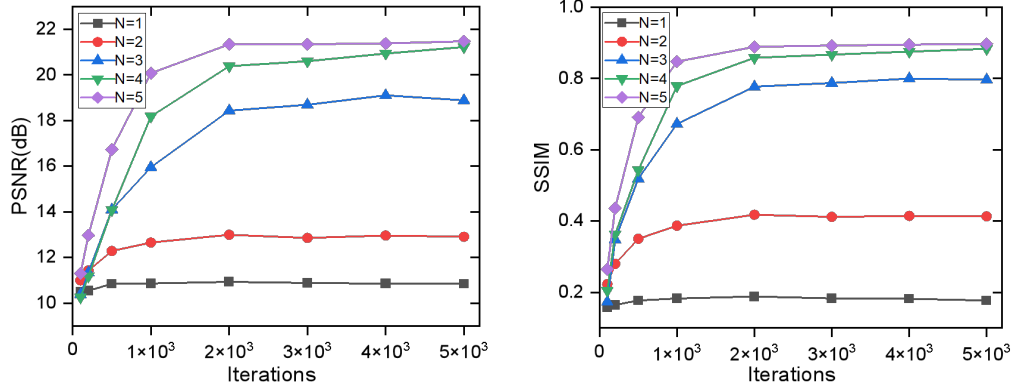


Fig. 4. Image quality metrics (PSNR and SSIM) of NeOTF reconstruction results under different input frame numbers  $N$  and iteration rounds from 100 to 5000. The metrics are calculated from the average of the reconstruction results of 5 frames.

Fig.3(b) shows the object reconstruction and phase error  $\Delta\phi_S$  between the real phase  $\phi_S$  and estimated phase  $\phi'_S$  of the NeOTF algorithm when the input is 1 to 5 frames of speckles. For low-frequency areas that have a greater impact on the image, the NeOTF fitting effect is better than that for high-frequency areas. According to the VCZ theorem [39], for a finite circular aperture, the OTF can be approximated as the autocorrelation of the aperture function. At this time, the MTF at low frequencies is higher, so the OTF phase at low frequencies has a more significant impact on the image. The PSNR and SSIM of NeOTF under different input frame numbers  $N$  and different iteration numbers are shown in the Fig.4. The imaging quality of NeOTF reaches convergence at 2000 iterations. As the number of input redundant frames increases, the retrieval accuracy and imaging quality of NeOTF increase, and it basically converges when the input frame number  $N = 5$ . And when  $N$  is greater than 3, continuing to increase the number of

redundant speckle frames has little effect on the imaging quality, indicating that NeOTF has been applied sufficient physical constraints to retrieve the phase of OTF.

### 3.2. Experiments

The experimental setup of non-invasive imaging through static scattering medium is shown in Fig.5. We used a He-Ne laser with a wavelength of 632.8 nm to generate pseudo-thermal light source. We used a DMD (Digital Micromirror Device, FLDISCOVERY F4100 0.7XGA,  $1024 \times 768$  pixels, pixel size  $13.68 \times 13.68 \mu\text{m}$ ) to load a certain number of objects at fixed intervals. The DMD was placed at a distance of  $u = 635 \text{ mm}$  from the scattering medium. We used a 220 grit ground glass as the scattering medium and place a 8mm diameter aperture before it. The camera (Daheng-imaging MER-2000-19U3M,  $5496 \times 3672$  pixels with a pixel size of  $2.4 \times 2.4 \mu\text{m}$ ) was placed  $v = 100 \text{ mm}$  from the diffuser to capture speckle images after being scattered by the ground glass. The captured speckles were subjected to frequency filtering and Gaussian filtering to remove noise. Then we crop the central area of  $1024 \times 1024$  pixels and feed them to the reconstruction frameworks.

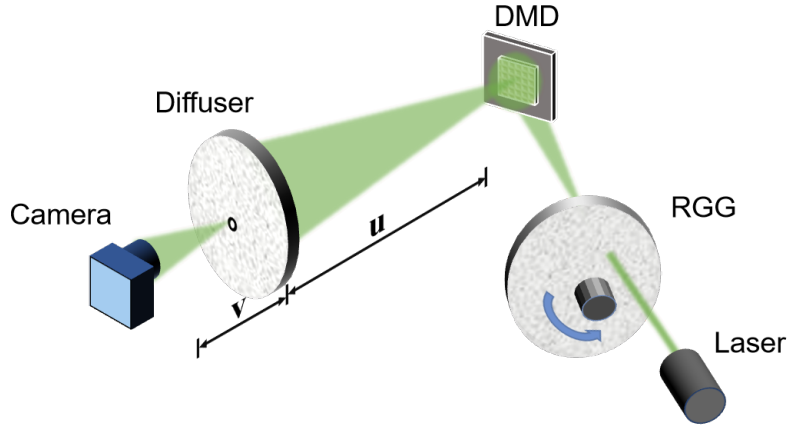


Fig. 5. The experimental setup of non-invasive imaging through static scattering medium. RGG is the rotating groundglass, which is used to generating pseudothermal light source. The pattern of objects are loaded on the DMD, reflecting the light to static diffuser.

Fig.6 presents a comparison of the final reconstruction results. The Hybrid Input-Output (HIO) algorithm and a baseline Untrained Neural Network both performed reconstructions using only the power spectrum derived from a single speckle frame. In contrast, the *MORE* algorithm and our proposed NeOTF both utilized five speckle frames to retrieve the full OTF, subsequently reconstructing the image via inverse filtering.

Qualitatively, the HIO reconstruction captures the object's basic structure but suffers from significant noise and non-uniform brightness artifacts. While the Untrained Neural Network produces a smoother result, attributable to its convolutional decoder architecture, it fails to recover the correct structural details. Both *MORE* and NeOTF successfully restore the object's structure; however, the reconstruction from NeOTF exhibits demonstrably lower noise levels and enhanced structural clarity. This comparison indicates that NeOTF's neural optimization strategy yields more accurate and robust results than the conventional error-reduction algorithm employed by *MORE*.



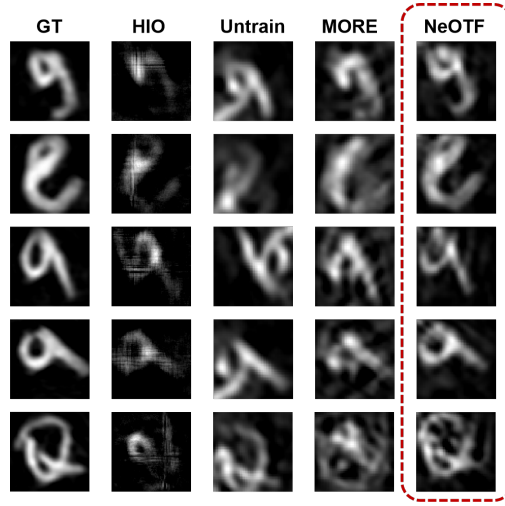


Fig. 6. Experimental results of reconstruction of different algorithm with the same speckles captured in the experiments.

### 3.3. Discussion

NeOTF surpasses the untrained neural network and traditional nonlinear optimization phase retrieval algorithms in imaging quality based on the physical constraints of multi-frame speckle and the neural network optimization algorithm. With the retrieved OTF, objects can be reconstructed by a simple inverse-filtering. The imaging process of NeOTF has high temporal resolution and efficiency, and does not require a guide-star or additional optical components like wavefront-shaping based technique.

Similar to other neural representation methods, NeOTF can freely handle speckles of different sizes. The low efficiency of iterative training under large-scale speckle is a shortcoming of NeOTF. The phase of the OTF of a strong scattering system is usually a random-like phase map, which is difficult to encode by traditional methods such as Zernike polynomials. Therefore, NeOTF currently needs to recover the full-size phase map, which means that NeOTF needs to optimize millions of parameters at the same time. Its training speed is limited by the size of the input speckle. When the input size is too large, the optimization speed of the entire network will drop sharply. In order to improve imaging efficiency and practical applications, it may be necessary to optimize the network structure and explore the encoding method of random phase.

## 4. Conclusion

In conclusion, we proposed a non-invasive scatter imaging method based on implicit neural representation of OTF, NeOTF. It aims to improve the ability of neural networks to solve ill-posed problems by introducing strong physical constraints. Through both numerical simulations and experimental methods, we demonstrate that the proposed NeOTF can notably enhance the precision of phase retrieval and the quality of images by augmenting the quantity of input speckle frames. Without the need for guiding stars or invasive priors, this method can achieve efficient and high-quality image reconstruction in static scattering media.

## References

1. D. Faccio, A. Velten, and G. Wetzstein, “Non-line-of-sight imaging,” *Nat. Rev. Phys.* **2**, 318–327 (2020).
2. S. Yoon, M. Kim, M. Jang, *et al.*, “Deep optical imaging within complex scattering media,” *Nat. Rev. Phys.* **2**, 141–158 (2020).



3. O. Katz, E. Small, and Y. Silberberg, "Looking around corners and through thin turbid layers in real time with scattered incoherent light," *Nat. Photonics* **6**, 549–553 (2012).
4. T. Yeminy and O. Katz, "Guidestar-free image-guided wavefront shaping," *Sci. Adv.* **7**, eabf5364 (2021).
5. B. Y. Feng, H. Guo, M. Xie, *et al.*, "Neuws: Neural wavefront shaping for guidestar-free imaging through static and dynamic scattering media," *Sci. Adv.* **9**, eadg4671 (2023).
6. F. Xia, I. Leite, R. Prevedel, and T. Chaigne, "Optical wavefront shaping in deep tissue using photoacoustic feedback," *J. Physics: Photonics* **6**, 043005 (2024).
7. S. M. Popoff, G. Lerosey, R. Carminati, *et al.*, "Measuring the transmission matrix in optics: An approach to the study and control of light propagation in disordered media," *Phys. Rev. Lett.* **104**, 100601 (2010).
8. D. Andreoli, G. Volpe, S. Popoff, *et al.*, "Deterministic control of broadband light through a multiply scattering medium via the multispectral transmission matrix," *Sci. Reports* **5**, 10347 (2015).
9. A. Velten, T. Willwacher, O. Gupta, *et al.*, "Recovering three-dimensional shape around a corner using ultrafast time-of-flight imaging," *Nat. Commun.* **3**, 745 (2012).
10. C. Wu, J. Liu, X. Huang, *et al.*, "Non-line-of-sight imaging over 1.43 km," *Proc. National Acad. Sci.* **118**, e2024468118 (2021).
11. J. Bertolotti, E. G. Van Putten, C. Blum, *et al.*, "Non-invasive imaging through opaque scattering layers," *Nature* **491**, 232–234 (2012).
12. O. Katz, P. Heidmann, M. Fink, and S. Gigan, "Non-invasive single-shot imaging through scattering layers and around corners via speckle correlations," *Nat. Photonics* **8**, 784–790 (2014).
13. J. R. Fienup, "Phase retrieval algorithms: a comparison," *Appl. Opt.* **21**, 2758–2769 (1982).
14. M. Hofer, C. Soeller, S. Brasselet, and J. Bertolotti, "Wide field fluorescence epi-microscopy behind a scattering medium enabled by speckle correlations," *Opt. Express* **26**, 9866–9881 (2018).
15. D. Lu, Q. Xing, M. Liao, *et al.*, "Single-shot noninvasive imaging through scattering medium under white-light illumination," *Opt. Lett.* **47**, 1754–1757 (2022).
16. M. Liao, D. Lu, W. He, *et al.*, "Improving reconstruction of speckle correlation imaging by using a modified phase retrieval algorithm with the number of nonzero-pixels constraint," *Appl. Opt.* **58**, 473–478 (2019).
17. W. Li, B. Wang, T. Wu, *et al.*, "Lensless imaging through thin scattering layers under broadband illumination," *Photonics Res.* **10**, 2471–2487 (2022).
18. S. Zheng, M. Liao, F. Wang, *et al.*, "Non-line-of-sight imaging under white-light illumination: a two-step deep learning approach," *Opt. Express* **29**, 40091–40105 (2021).
19. J. Li, Z. Zhang, M. Huang, *et al.*, "Non-invasive imaging through scattering media with unaligned data using dual-cycle gans," *Opt. Commun.* **525**, 128832 (2022).
20. F. Wang, Y. Bian, H. Wang, *et al.*, "Phase imaging with an untrained neural network," *Light. Sci. & Appl.* **9**, 77 (2020).
21. Z. Tang, F. Wang, Z. Fu, *et al.*, "Deepsci: scalable speckle correlation imaging using physics-enhanced deep learning," *Opt. Lett.* **48**, 2285–2288 (2023).
22. Y. Shi, E. Guo, M. Sun, *et al.*, "Non-invasive imaging through scattering medium and around corners beyond 3d memory effect," *Opt. Lett.* **47**, 4363–4366 (2022).
23. F. Liu, X. Meng, Y. Yin, and X. Yang, "Imaging through a scattering medium via model-driven deep learning," *Opt. Lett.* **48**, 5285–5288 (2023).
24. H. Wang, J. Zhu, Y. Li, *et al.*, "Neuph: scalable and generalizable neural phase retrieval with local conditional neural fields," *Adv. Photonics Nexus* **3**, 056005–056005 (2024).
25. Q. Chen, C.-t. Cai, X.-t. He, and R. Chen, "Fourier ptychographic microscopy with a two-stage physics-enhanced neural network," *Opt. Laser Technol.* **181**, 112016 (2025).
26. Z. Fu, F. Wang, Z. Tang, *et al.*, "Adaptive imaging through dense dynamic scattering media using transfer learning," *Opt. Express* **32**, 13688–13700 (2024).
27. V. Sitzmann, J. Martel, A. Bergman, *et al.*, "Implicit neural representations with periodic activation functions," *Adv. Neural Inf. Process. Syst.* **33**, 7462–7473 (2020).
28. M. Hui, Z. Wei, H. Zhu, *et al.*, "Microdiffusion: Implicit representation-guided diffusion for 3d reconstruction from limited 2d microscopy projections," in *Proceedings of the IEEE/CVF Conference on Computer Vision and Pattern Recognition*, (2024), pp. 11460–11469.
29. T. Chien, R. Cao, F. L. Liu, *et al.*, "Space-time reconstruction for lensless imaging using implicit neural representations," *Opt. Express* **32**, 35725–35732 (2024).
30. H. Zhou, B. Y. Feng, H. Guo, *et al.*, "Fourier ptychographic microscopy image stack reconstruction using implicit neural representations," *Optica* **10**, 1679–1687 (2023).
31. T. Wu, J. Dong, and S. Gigan, "Non-invasive single-shot recovery of a point-spread function of a memory effect based scattering imaging system," *Opt. Lett.* **45**, 5397–5400 (2020).
32. H. Tu, H. Liu, T. Pan, *et al.*, "Deep empirical neural network for optical phase retrieval over a scattering medium," *Nat. Commun.* **16**, 1369 (2025).
33. Y. Yuan and H. Chen, "Dynamic noninvasive imaging through turbid media under low signal-noise-ratio," *New J. Phys.* **22**, 093046 (2020).
34. S. Mukherjee, A. Vijayakumar, M. Kumar, and J. Rosen, "3d imaging through scatterers with interferenceless optical system," *Sci. Reports* **8**, 1134 (2018).

35. M. Tancik, P. Srinivasan, B. Mildenhall, *et al.*, “Fourier features let networks learn high frequency functions in low dimensional domains,” *Adv. Neural Inf. Process. Syst.* **33**, 7537–7547 (2020).
36. D. Ulyanov, A. Vedaldi, and V. Lempitsky, “Deep image prior,” in *Proceedings of the IEEE conference on computer vision and pattern recognition*, (2018), pp. 9446–9454.
37. K. C. Zhou and R. Horstmeyer, “Diffraction tomography with a deep image prior,” *Opt. Express* **28**, 12872–12896 (2020).
38. O. Ronneberger, P. Fischer, and T. Brox, “U-net: Convolutional networks for biomedical image segmentation,” in *Medical image computing and computer-assisted intervention–MICCAI 2015: 18th international conference, Munich, Germany, October 5-9, 2015, proceedings, part III 18*, (Springer, 2015), pp. 234–241.
39. J. W. Goodman, *Speckle phenomena in optics: theory and applications* (Roberts and Company Publishers, 2007).